JAAS

PAPER

View Article Online
View Journal | View Issue

Cite this: J. Anal. At. Spectrom., 2023, 38, 873

Multi-element signal enhancement mechanism investigation for laser ablation-assisted ultraviolet laser excited atomic fluorescence†

Kaikai Kou,[ab] Weiran Song,[ab] Weilun Gu,[ab] Jiacen Liu,[ab] Yuzhou Song,[ab] Jianxun Ji,[ab] Zongyu Hou[ab] and Zhe Wang *[ab]

Multi-element detectable laser excited atomic fluorescence (LEAF) technique has been regarded as impressive progress in the analytical field because it possesses high sensitivity and overcomes the specific resonant wavelength constraint. However, a limited understanding of the universal signal enhancement mechanism restricts its further development and follow-up studies. In this study, experiments of LEAF are conducted to investigate the details of the ablation process, excitation process, and coupling behavior. Multi-element signals were dramatically enhanced with 1.49 mJ ablation laser energy at t_{ip} = 200 ns, and quantitative analysis with minimal destruction was obtained. Compared with the literature, the following new understandings are firstly proposed: (1) the ablated mass from the ablation process was plasma instead of just a plume, which was stimulated by an excitation laser; (2) photoexcitation contributes to the enhanced signal other than the electron thermal excitation supported by the fact that the signal gains its higher intensity when the re-excited plasma was less bright. That is, the multi-element excitation may relate to the atom energy-level distortion by the electric field. With the elucidation of key processes and mechanisms, there would be a much broader application for laser ablation-assisted ultraviolet LEAF due to its distinctive advantages.

Received 4th January 2023
Accepted 21st February 2023

DOI: 10.1039/d3ja00002h

rsc.li/jaas

1. Introduction

Laser-induced breakdown spectroscopy (LIBS) is a powerful detection technology that plays a key role in the atomic spectroscopy family.[1–3] Its good capabilities of rapid, *in situ*, multi-element analysis and minimal sample preparation have been successfully demonstrated in many fields, such as coal utilization,[4–6] geochemistry,[7] metallurgy industries,[8] and cultural heritage.[9] Despite its increasing popularity, the quantitative performance of LIBS often cannot meet the detective requirements due to its modest sensitivity and precision.[10,11] The laser-excited atomic fluorescence of plume, plume-LEAF for short, first proposed by Cheung *et al.*, possesses high sensitivity and its excellent analytical performance has been demonstrated.[12,13]

The typical setup of plume-LEAF is a two-laser pulse scheme. The first laser, the ablation laser pulse is focused on the sample surface to ablate a small amount of the material. Then, the expanding material is intercepted by the excitation laser, in which an ultraviolet (UV) laser is normally employed.[13] When the species are excited by the UV photon, signals of various elements are enhanced hundreds of times. Cheung *et al.* stimulated the fluorescence of several elements in aluminum alloys with an ArF excimer laser and obtained sensitivity orders of magnitude higher than that in LIBS.[14,15] Since less sample mass is required for the detectable signal, lower ablation laser energy is employed and the sample is going to be minimally destructed. Thus, metal segregation is prevented, which made depth profiling possible.[16] This technique is also capable of detecting various elements in different kinds of samples, such as stainless steel, ceramics, and polymer.[14,17–19] Moreover, in the artwork analysis, which has to be almost nondestructive, plume-LEAF is able to detect the minor and trace signature elements in the ink.[20] Therefore, sensitive, minimally destructive, and multi-elemental analysis was achieved in this technique.

Although the impressive capability of plume-LEAF appeals to great interest,[1,21,22] until now, there is no report on other researchers successfully repeating the outstanding results, except for Prof. Cheung's group because of the lack of a convincing mechanism. To interpret the behavior of the unselective signal enhancement, Cheung *et al.* proposed a plausible dense plume model based on the experiment phenomenon.[13,23] Based on the generally applied low ablation

[a]State Key Lab of Power Systems, International Joint Laboratory on Low Carbon Clean Energy Innovation, Department of Energy and Power Engineering, Tsinghua University, Beijing, 100084, China. E-mail: zhewang@tsinghua.edu.cn

[b]Shanxi Research Institute for Clean Energy, Tsinghua University, Taiyuan, 030032, China

† Electronic supplementary information (ESI) available: Appendixes: supplementary material is attached. See DOI: https://doi.org/10.1039/d3ja00002h

laser energy, the authors assumed that the ablation laser just created a vapor plume without igniting the ionized plasma. The plume refers to the flow of two fluids with a density difference,[24] from which the name came. The species embedded in the nascent plume had high density in a short delay time (about 60 ns). Therefore, the electron energy levels broadened and smeared with each other to form the band-like structure resulting in unnecessary specific wavelengths of the excitation laser and broadening the spectra.[14,25] However, some detailed processes in plume-LEAF are still unclear, which will be further discussed in the following paragraphs. Therefore, it is difficult to summarize the key processes to repeat the experiment results.

The two laser pulses are supposed to cleverly couple with each other. The basic procedure of plume-LEAF consists of two laser pulses, corresponding to the ablation process and the excitation process, respectively. It is of great importance to further investigate the mechanism and to elucidate the key processes enabling the plume-LEAF phenomenon. Firstly, in the ablation process, whether it is plume or plasma still has not been studied, which is affected by many factors, such as laser parameters, focal conditions, and material properties.[26,27] When the fluence of the ablation laser is below the ionization threshold, the ablated mass is only the vapor plume without free electrons.[24] If the energy of ablation laser is sufficient to overcome the threshold, plasma generated. In the early stage of plasma, the broadened spectral may be a consequence of stark broadening and self-absorption.[28] The product of the ablation process, which is closely related to the subsequent process, is still confusing. Thus, the name of the technique will be changed to LEAF in the following discussion.

Secondly, in the excitation process, there are some experimental phenomena inconsistent with the dense plume model. If an energy level is broadened to some extent, for example, $\pm$0.5 eV, the emission line with the upper energy level near 6.4 eV (photon energy of 193 nm laser) is supposed to have priority to be enhanced. But in the experiment from ref. 23, the intensity of Cu 510.55 nm was higher than that of Cu 515.32 nm. The study and application of LEAF are hindered by the confusing mechanism interpretation. Moreover, the geometrical configuration of the LEAF experiment setup is similar to the reheating double-pulse (DP) LIBS. The multi-element signal enhancement behavior by single wavelength UV-photon is similar to the intense electron-impact excitation (thermal excitation), which relies on the local high temperature of electrons.[29–31] Therefore, the excitation process needs to be further characterized to obtain a convincing mechanism.

The present work makes efforts to repeat the LEAF phenomenon and unveil the underlying details of the ablation process and excitation process. The effect of the experimental parameters on the process's coupling behavior was demonstrated on a brass sample. Then, for a better fundamental understanding of the two key processes, spectra at different delay times and time-resolved plasma images were obtained. Finally, based on the results, a new perspective for explaining signal enhancement is proposed.

2. Experiments

2.1 Samples

Considering the multi-element components, the alloys, standard brass samples from the Central Iron and Steel Research Institute (CISRI) of China, were employed, which are commercially available and calibrated accurately, as shown in Table 1. The samples were machined into a column billet of 38 mm diameter and 10 mm height. Before the test, the sample was polished with sandpaper (1500 mesh per inch) and then cleaned with ethanol to make the surface smooth. The sample ZBY901 was used to demonstrate the effect of experiment conditions, other samples were only used to establish a calibration curve.

2.2 Experimental setup

The experiment system is schematically shown as Fig. 1. A Q-switched Nd:YAG laser pulse (Quantel, CFR, 1064 nm, 1 Hz), with a pulse duration of 8.4 ns, beam diameter of 4.55 mm, maximum energy of 200 mJ, was introduced as the ablation laser. It was focused with a plano-convex lens of 50 mm (lens 1) vertically onto the flat surface of the sample for ablation. The sample was on an electric translation stage to avoid repetitively ablating the same area. The lens was intentionally placed about 46 mm above the sample surface. The ablation laser beam passed a variable attenuator to adjust the laser energy (E_a).

After a certain inter-pulse delay time (t_{ip}), an ArF excimer laser pulse (Coherent, Compex 201, 193 nm, 1 Hz, 20 ns) was triggered as the excitation laser. It was defocused with a plano-convex lens of 100 mm (lens 2) to horizontally intercept the plasma and re-excite the species. The rectangular excimer laser beam was 21 $\times$ 10 mm. Beam divergence was 0.4 $\times$ 0.4 mrad. The beam was reshaped by a diaphragm. The distance from the plasma to the lens was about 80 mm with a defocused spot size of about 2 $\times$ 1 mm, in which the short side was parallel to the sample surface. The energy of the excitation laser (E_e) was 0.6 mJ.

In order to ensure the light-collecting efficiency, a double-lens group was arranged. Then, the signal was guided by an optical fiber into a two-channel spectrometer (Avantes, AvaSpec-Dual) to obtain the emission spectra. The resolution was 0.07 nm. For the time-integrated spectra, the spectrometer was turned on about 1 μs earlier than the ablation laser. The gate width was the default value for the CCD instrument in the spectrometer, 1.05 ms. To monitor the plasma evolution, its image was acquired horizontally by an sCMOS camera (iStar sCMOS, Andor, UK) with a two-lens imaging unit. A broad

Table 1 The major components of the samples

Sample no.	Cu (%)	Pb (%)	Zn (%)	Fe (%)
ZBY901	73.00	2.77	23.99	0.028
ZBY902	64.43	1.87	33.45	0.036
ZBY903	60.28	0.766	38.79	0.047
ZBY904	59.14	1.50	38.85	0.167
ZBY906	56.62	0.581	41.76	0.037

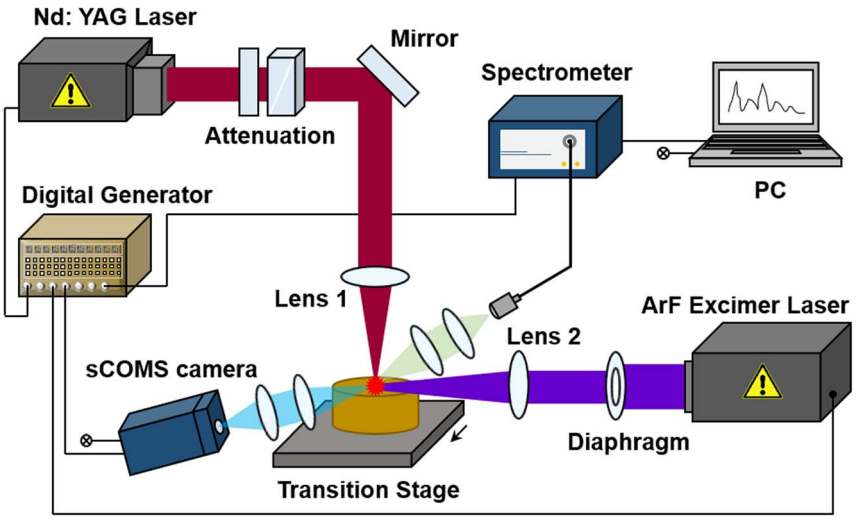

Fig. 1 Schematics of the LEAF scheme experimental system.

bandpass filter with high transmission in the visible region (400–800 nm) was placed just before the camera to avoid the irradiation of the laser. Imaging of Cu, Pb, and continuum radiation was performed by inserting a narrow bandpass filter centered at 510 nm (bandwidth FWHM ~ 10 nm), 400 nm (bandwidth FWHM ~ 40 nm), and 420 nm (bandwidth FWHM ~ 10 nm), respectively, between the broad bandpass filter and the camera. A digital generator (DG645, Stanford Research Systems, USA) was used to synchronize the system.

2.3 Data processing

Each displayed spectrum was the average of 60 pulses. The peak intensity of the spectrum was regarded as the signal intensity because of the ignorable background. The noise was defined as the standard deviation of the regions of 485–508 nm. The displayed plasma image was the average of 20 pulses and then smoothed with a 9 × 9 pixel sliding average.

3. Results and discussion

3.1 Coupling of the ablation and excitation process

The LEAF spectrum was produced by a 193 nm laser intercepting the 1064 nm-laser ablated plasma, while the LIBS spectrum was generated by the ablation laser alone. For the purpose of minimally destructive analysis, the ablation laser energy (E_a) was gradually decreased. When the LIBS signal disappeared, the intensity of the characteristic lines in the LEAF spectrum remained at a high level, as shown in Fig. 2. When the excitation laser was introduced, the intensities of Cu 510.55 nm, 515.32 nm, and 521.82 nm were dramatically enhanced to ~500, 100, and 170 in CCD counts, respectively. While the enhancement of Zn emission lines was insignificant. The emission of the minor element, Pb 405.78 nm, was greatly elevated. It seemed that 193 nm photons preferred to excite Pb species as was demonstrated in previous studies.[12,13] Nevertheless, the background of the LEAF spectrum was negligible. The noise for both spectra was about 39 in CCD counts. Compared with previous work, the spectra shape, such as background intensity and relative intensity of Cu emissions, was consistent with that in ref. 23. Therefore, the LEAF phenomenon was repeated.

Then, the coupling behavior of the ablation and excitation process was investigated by revealing the influence of the key experimental parameters, ablation laser energy (1.02–3.53 mJ), and inter-pulse delay time (0–1500 ns), as shown in Fig. 3. At the bottom left, the LIBS spectra intensity and the same symbol represents the same E_a. For Cu 510.55 nm, with E_a increasing, more target atoms were ablated resulting in the increased LEAF signal. But the signal enhancement amplitude of LEAF compared to LIBS decreased with increasing E_a.

There was an optimal t_{ip} for Cu emission and the t_{ip} was delayed with increasing E_a. At the beginning of the nascent plasma, the electron density was high and the excitation laser was mainly absorbed by electrons. It may relate to the thermal excitation when t_{ip} was 0 ns. When electrons died out, the

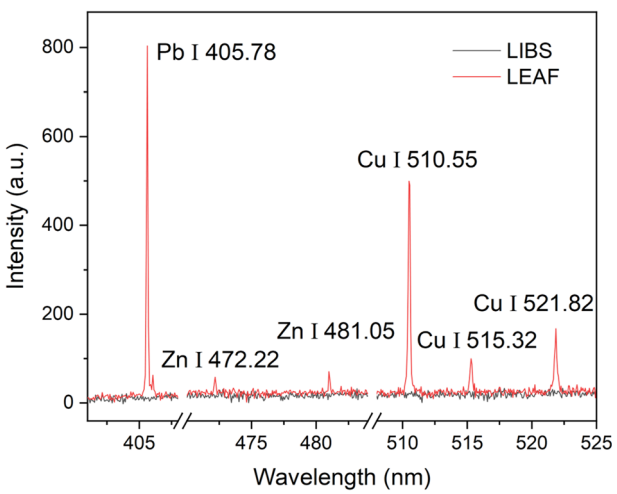

Fig. 2 The spectra of LIBS and LEAF scheme. E_a = 1.49 mJ, E_e = 0.6 mJ. t_{ip} = 200 ns.

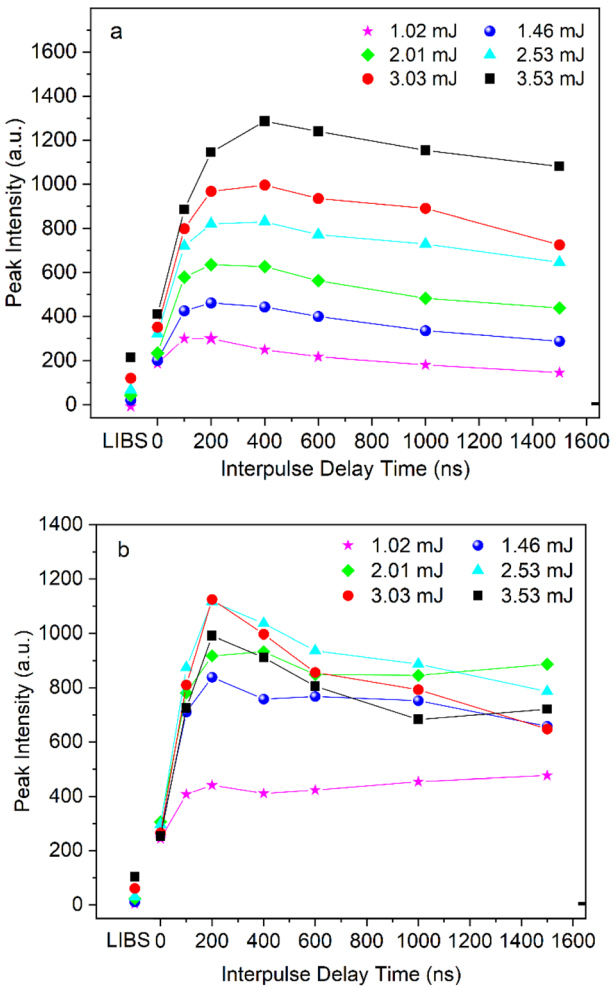

Fig. 3 Effect of ablation laser energy and inter-pulse delay (t_{ip}) on spectra intensity. E_e = 0.6 mJ. (a) Cu 510.55 nm; (b) Pb 405.78 nm.

absorbance of the excitation laser was dominated by atoms resulting in an enhanced signal. With the plasma further expanding, the atom density decreased in the viewing zone, and the signal intensity declined.[18] For Pb 405.78 nm, the optimal E_a and t_{ip} were about 2.53 mJ and 200 ns, respectively. When E_a was higher than the optimal value, high electron density may prevent the excitation of Pb atoms.

Compared to the typical LIBS detection system, LEAF can remarkably reduce the ablation energy with detectable signals, as shown in Fig. S1†.[32] More detailed information on emission intensity and relative standard deviation (RSD) of Cu 510.55 nm and Pb 405.78 nm in different ablation energy and inter-pulse delay time is displayed in Fig. S2 and S3.† The RSD of Cu emission was about 10% when the ablation laser energy was 1.46 mJ. So, it has great potential for LEAF to realize the quantitative analysis of minimal destruction.

3.2 Quantitative analysis performance of LEAF

To evaluate the quantitative analysis capability, calibration curves were established on the brass samples, as shown in Table 1. The most intensified emission lines in Fig. 2, Cu 510.55 nm and Pb 405.8 nm, were adopted as the analytical lines. Fig. 4 shows the peak intensity *versus* the concentration, and the standard deviation is represented by error bars. Higher ablation laser energy led to better performance analysis of Cu, as shown in Fig. 4(a) and (b). Satisfying quantitative performance was obtained when E_a was 1.49 mJ, in which R^2 was 0.915 and 0.950 for Cu and Pb in the LEAF scheme, respectively. Pb was more sensitive in the LEAF scheme than Cu and a better linear correlation was observed. In order to compare the performance of LEAF and LIBS, LIBS experiments were conducted at higher ablation energy, E_a = 4.48 mJ. Although the intensity of the emission lines was similar, the linear correlation of the concentration and peak intensity was poor. It also needs to be mentioned that LIBS was more destructive.

In order to fully reveal the extent of destruction in LIBS and LEAF scheme, the ablation crater was imaged with confocal microscopy under a 10× objective lens, as shown in Fig. 5. The fluence distribution in the focal plane was influenced by focal condition and laser beam parameters. For counting the overall irradiated area, the diameter was measured on the crater in the LIBS scheme, 4.51 mJ, 20 pulses, which was about 750 μm. The ablation energy density of LEAF was 233 mJ cm^{-2} and 330 mJ cm^{-2} at 1.03 mJ and 1.46 mJ, respectively. At such low laser fluence, only a small mass of the sample was removed. The crater was generated by 20 pulses for easy observation. The enhanced signal was not originated from the mass increment in LEAF scheme because of the similar crater within which the LIBS scheme under the same ablation energy. When the ablation energy increased, the crater grew larger and deeper, especially at 4.51 mJ.[33,34]

In the LIBS scheme, sufficient laser energy needs to be applied to overcome the ablation and ionization thresholds. For a detectable signal, the energy is supposed to be higher than the detection threshold, as shown in Fig. 6.[35] High ablation energy results in increased ablation mass. In addition, there is inadvertent removal of the more unexcited ablate material ejected by the expending vapor.[32] While in the LEAF scheme, with the assistance of an excitation laser, ablation laser energy can be reduced below the detection threshold of LIBS. Therefore, the ablation laser energy and the mass removal can be significantly reduced. With the advantage of low absolute LOD, LEAF provided a viable solution for the elemental analysis of valuable objects and scarce specimens.[36,37]

3.3 Characterization of the ablation process

To study the ablation process, the ablated mass was directly observed by the time-resolved image in LIBS and LEAF scheme, as shown in Fig. 7. The pictures in a dashed frame shared the same color bar. It was clearly demonstrated that the ablated sample was luminous and ionized. The evolution of plasma was tracked. The duration time of plasma was about 1000 ns.[38,39] When the excitation laser was introduced transversely, the position and morphology of plasma were barely changed in the LEAF scheme. It is different from the traditional orthogonal double pulse LIBS, in which another plasma was induced in the core area by the second laser.[40,41] But the plasma was ignited

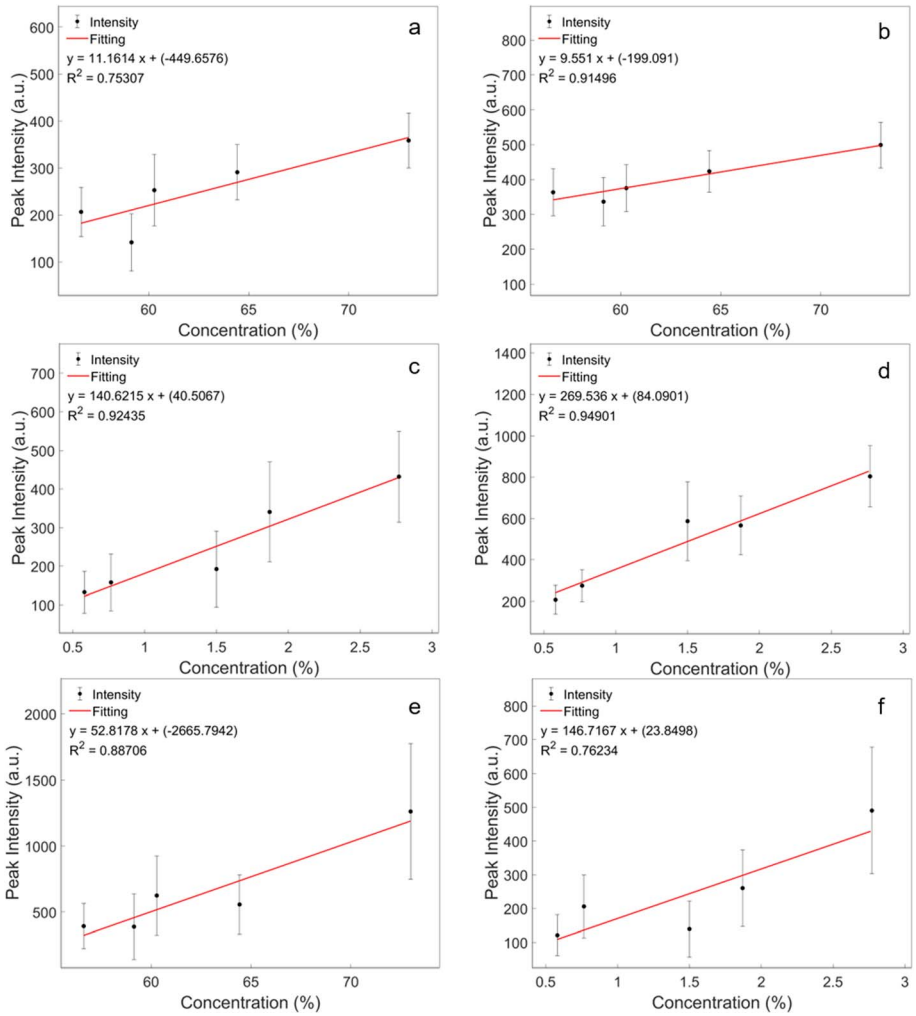

Fig. 4 Calibration curve for brass sample analysis. LEAF spectra of Cu 510.55 nm, $t_{ip} = 200$ ns, (a) $E_a = 1.02$ mJ, (b) $E_a = 1.49$ mJ. LEAF spectra of Pb 405.78 nm, $t_{ip} = 200$ ns, (c) $E_a = 1.02$ mJ, (d) $E_a = 1.49$ mJ. LIBS spectra at $E_a = 4.48$ mJ, € Cu 510.55 nm, (f) Pb 405.78 nm.

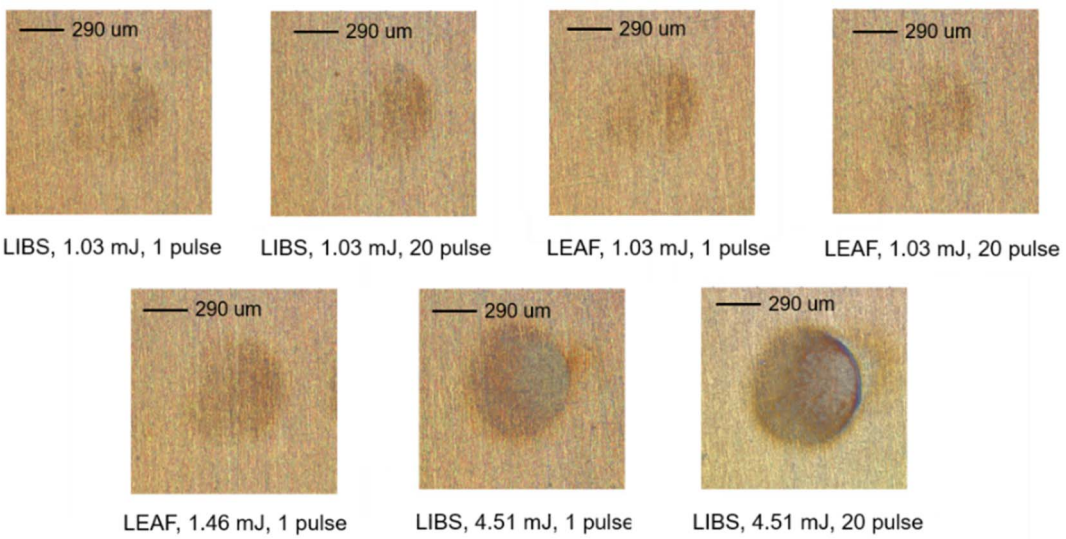

Fig. 5 Confocal microscopic image of ablation craters.

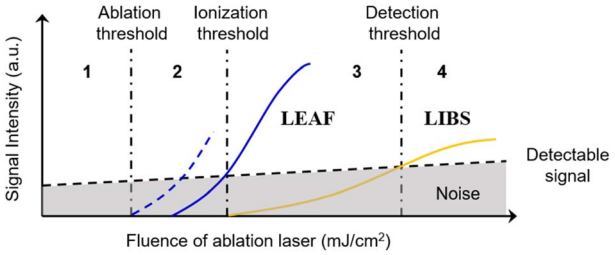

Fig. 6 Schematic of the relationship of signal intensity and ablation laser fluence in LIBS and LEAF scheme.

again and became brighter. Then, the bright plasma decayed rapidly within ~200 ns, especially in the central area.

According to the dense plume model,[13,23] the pre-condition of the ablation process enabling the LEAF phenomenon should make the ablation laser lower than the ionization threshold, as the blue dashed line suggested in Fig. 6. However, the results indicated that it should overcome the ionization threshold, and the ablated mass was plasma instead of plume, as shown by the blue solid line in Fig. 6.

3.4 Characterization of the excitation process

In order to explicitly reveal the details of the excitation process, the spectra, and plasma images were collected. The spectrometer was controlled at a certain delay time relative to the excitation laser and the spectra were time integrated at each delay to estimate the signal lifetime, as shown in Fig. 8. The LEAF spectra of Cu and Pb optical emission lines were closely accompanied by the excitation laser. The duration of all the emission lines was very short, only about 80 ns.

As can be seen in Fig. 3, the signal enhancement of LEAF at an inter-pulse delay time of 0 ns was less significant than at 200 ns. The reason was further explored by imaging the plasma of LEAF at different inter-pulse delay times, which is shown in Fig. 9. Although the plasma was ignited brighter when t_{ip} was 0 ns, the signal was elevated to a higher level when t_{ip} was 100 ns or 200 ns. Therefore, the signal enhancement mechanism of LEAF is quite different from that of the reheating double pulse LIBS since the latter mainly originated from higher plasma temperature.[42,43]

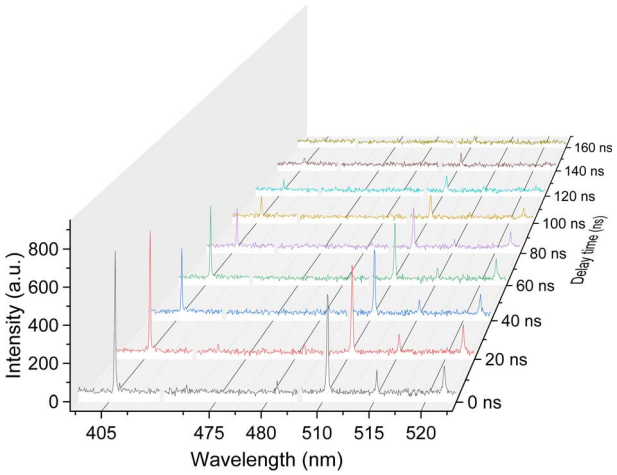

Fig. 8 Time-integrated spectra at each delay of LEAF. $E_a = 1.5$ mJ, $t_{ip} = 200$ ns. An excitation laser was induced at 0 ns of the graph.

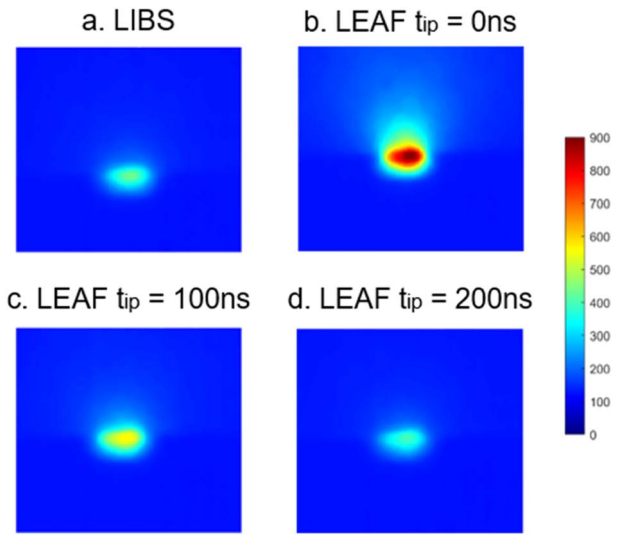

Fig. 9 Plasma image of LIBS (relative to ablation laser) and LEAF (relative to excitation laser), through the broad bandpass filter. The gate delay time of all pictures is 0 ns. Gate width 100 ns; $E_a = 1.5$ mJ; t_{ip} for LEAF scheme was labeled.

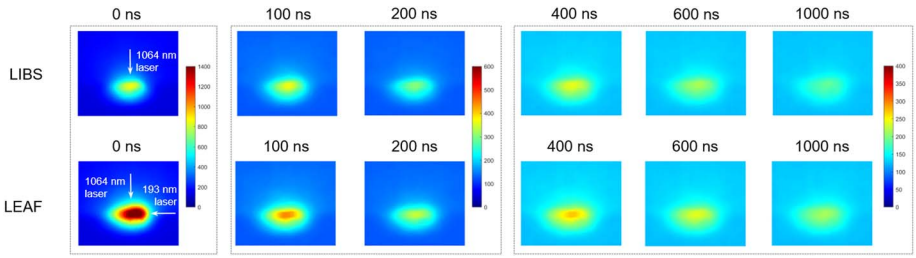

Fig. 7 Plasma image evolution with a delay time of LIBS (relative to ablation laser) and LEAF (relative to excitation laser), through the broad bandpass filter. The delay time was labeled on the graph. Gate width was 100 ns; $E_a = 1.5$ mJ; $t_{ip} = 200$ ns for LEAF scheme.

In the excitation process, there is a question as discussed in the introduction section how to simultaneously enhance the multi-element signals of the LEAF scheme. Firstly, the signal enhancement is unlikely due to the broadband of the excimer laser. In addition to the commonly used 193 nm laser, Cai *et al.* verified that the 213 nm laser was also sufficient to excite the fluorescence signal.[44] As such, when the deep ultraviolet phonon was introduced into the plume, the distinct wavelength constraint can be eliminated. Secondly, the universal signal enhancement was also different upon reheating the double-pulse LIBS relying on the thermal excitation because the brighter plasma was accompanied by lower signal intensity, as shown in Fig. 9. According to previous studies, the signal should be attributed to the photoexcitation, which is independent on the electron temperature and LTE condition.[23,45]

In addition, the plasma was imaged with a narrow bandpass filter, as shown in Fig. 10. The gate delay time was 0 ns, which was relative to the ablation laser in the LIBS scheme and the

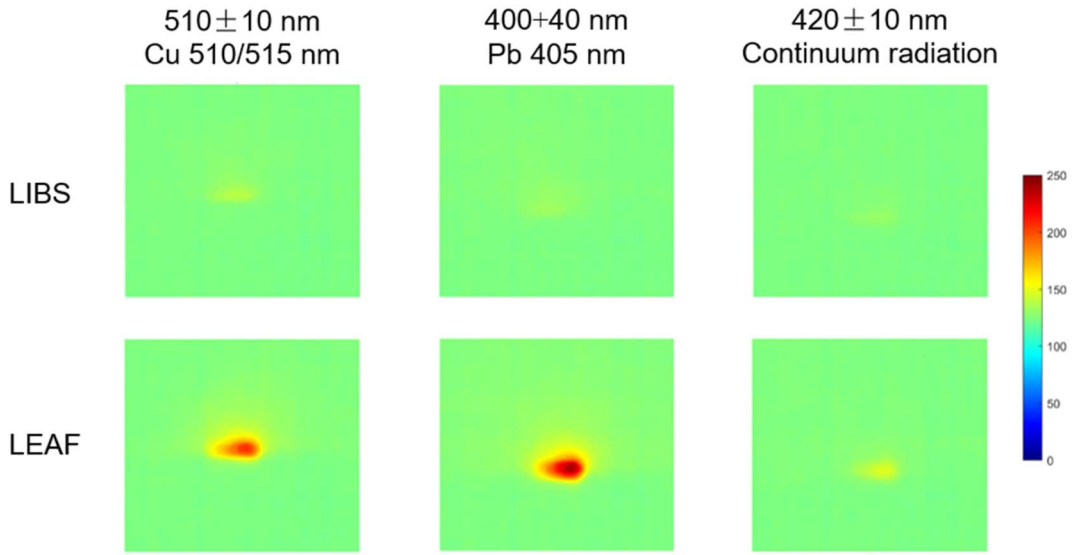

Fig. 10 Plasma image with a bandpass filter of LIBS (relative to ablation laser) and LEAF (relative to excitation laser), accompanied with the broad bandpass filter (400–800 nm). Gate delay 0 ns; Gate width 100 ns; $E_a = 1.50$ mJ; t_{ip} was 200 ns for LEAF scheme.

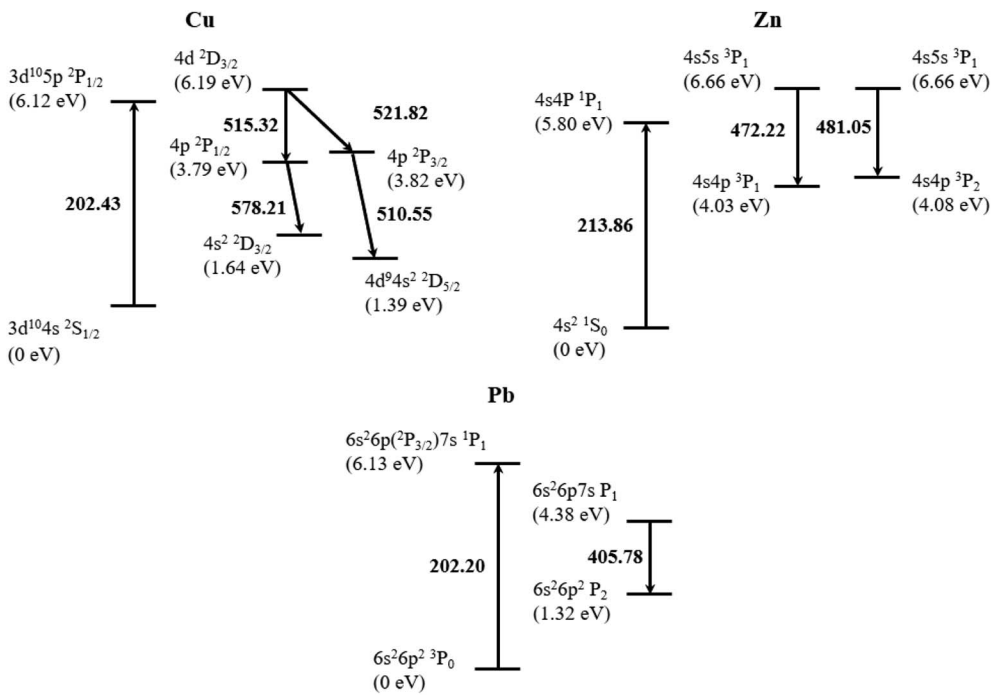

Fig. 11 Partial Grotrian diagrams of transitions of Cu, Zn, and Pb for reference.

excitation laser in the LEAF scheme. The parameters are labeled in the pictures. The continuum radiation was defined by the wavelength range of 410 nm to 430 nm. The background was not efficiently enhanced in the LEAF scheme. While the emissions of Pb and Cu were dramatically excited in a larger area than the continuous background radiation. Therefore, the photoexcitation process has priority to excite atoms than electrons.

Common transitions of the major elements in the target are shown in Fig. 11.[23] Some transitions were sufficiently populated as displayed in Fig. 2, while others were not. The transitions that originated from levels above 6.4 eV, such as the lines of Zn 481.05 nm and Zn 472.22 nm, were inefficiently excited. While the emissions at Cu 510.55 nm and Pb 405.78 nm dramatically enhanced with high efficiency than the lines at the higher upper energy levels, such as Cu 515.32 nm and Cu 521.82 nm. The plasma image in Fig. 9 suggested that it was not attributed to thermal excitation, which had a priority to stimulate the low energy levels when electron temperature was low. It was the photoexcitation that contributed to the intensified fluorescence signals.

From such results, the mechanism of universal signal enhancement behavior by single wavelength laser can be summarized. The product in the ablation process needs to be ready to be subsequently excited. As suggested in Fig. 7, the mass was ionized and free electrons were introduced in the ablation process. Thus, it is reasonable to speculate that the electrons played an important role in the LEAF excitation process and invoked the electric field mechanism. As the electric field of charged particles can decrease the ionization energy of atoms and ions, the electrons in the ablation product may change the energy-level structures of atoms to be made available to absorb the photons.[28,46] The energy levels around 4 eV were possible to be distorted and have priority to be induced to fluoresce. Because the breakdown phenomenon was captured by plasma image, it is inaccurate to describe the process with plume-LEAF. Thus, considering the compatibility of lasers at other ultraviolet wavelengths, it is reasonable to rename the technique as laser ablation-assisted ultraviolet LEAF. Up to now, there is barely any interpretation of the properties of plasma, and the LEAF technique may provide a new approach to probe the interaction of plasma and laser.

4. Conclusion

The experiment of LEAF was systematically conducted by employing a 193 nm laser to intercept the ablated plasma resulting in the dramatically enhanced fluorescence signals. The details of the key processes, which were essential to understanding the mechanism were demonstrated. For the Cu 510.55 nm line, the maximum intensity was obtained at an inter-pulse delay time of 200 ns when ablation energy was 1.46 mJ. Under the minimally destructive laser energy, the content of Cu and Pb can be quantitatively determined. More details were revealed in the ablation process and excitation process: (1) from the detailed spectra and images, the generation of plasma in the ablation process was firstly clarified instead of the plume; (2) the signal enhancement originated from photoexcitation other than thermal excitation. Moreover, the photoexcitation was supported by the following facts. Firstly, the signal has a short duration time, which was accompanied closely by the excitation laser. Secondly, the signal gained its higher intensity when the re-excited plasma was less bright. Thirdly, the atoms in the plasma were excited efficiently by the energetic ultraviolet photon in a larger zone compared to that of the electrons. Finally, the mechanism was discussed from a new perspective and the technique was renamed laser ablation-assisted ultraviolet LEAF.

The LEAF spectra possess the advantages of high signal-to-background ratio and simultaneous multi-element detection, which has great potential to be used in minimally or none destructive applications. Moreover, the interaction of ultraviolet photons and plasma may provide new diagnostic information about the nascent plasma.

Conflicts of interest

There are no conflicts to declare.

Acknowledgements

The authors are grateful for the financial support from the National Natural Science Foundation of China (No. 51906124), the Shanxi Province Science and Technology Department (20201101013), and the Scientific Research Program for Young Talents of China National Nuclear Corporation (2020).

References

1 Z. Wang, M. S. Afgan, W. Gu, *et al.*, Recent advances in laser-induced breakdown spectroscopy quantification: From fundamental understanding to data processing, *TrAC, Trends Anal. Chem.*, 2021, 143.
2 J. Laserna, J. M. Vadillo and P. Purohit, Laser-Induced Breakdown Spectroscopy (LIBS): Fast, Effective, and Agile Leading Edge Analytical Technology, *Appl. Spectrosc.*, 2018, **72**(1_suppl), 35–50.
3 Z. Wang, T.-B. Yuan, Z.-Y. Hou, *et al.*, Laser-induced breakdown spectroscopy in China, *Front. Phys.*, 2014, **9**(4), 419–438.
4 Z. Hou, Z. Wang, L. Li, *et al.*, Fast measurement of coking properties of coal using laser induced breakdown spectroscopy, *Spectrochim. Acta, Part B*, 2022, 191.
5 S. Sheta, M. S. Afgan, Z. Hou, *et al.*, Coal analysis by laser-induced breakdown spectroscopy: a tutorial review, *J. Anal. At. Spectrom.*, 2019, **34**(6), 1047–1082.
6 W. Song, Z. Hou, W. Gu, *et al.*, Industrial at-line analysis of coal properties using laser-induced breakdown spectroscopy combined with machine learning, *Fuel*, 2021, 306.
7 T. Chen, T. Zhang and H. Li, Applications of laser-induced breakdown spectroscopy (LIBS) combined with machine learning in geochemical and environmental resources exploration, *TrAC, Trends Anal. Chem.*, 2020, 133.

8 J. D. Pedarnig, S. Trautner, S. Grünberger, *et al.*, Review of Element Analysis of Industrial Materials by In-Line Laser—Induced Breakdown Spectroscopy (LIBS), *Appl. Sci.*, 2021, **11**(19), 9274.
9 A. Botto, B. Campanella, S. Legnaioli, *et al.*, Applications of laser-induced breakdown spectroscopy in cultural heritage and archaeology: a critical review, *J. Anal. At. Spectrom.*, 2019, **34**(1), 81–103.
10 W. Gu, Z. Hou, W. Song, *et al.*, Compensation for the variation of total number density to improve signal repeatability for laser-induced breakdown spectroscopy, *Anal. Chim. Acta*, 2022, **1205**, 339752.
11 W. Song, S. Zhao, Y. Zhang, *et al.*, Application of laser-induced breakdown spectroscopy and chemometrics for rapid identification of fire-retardant/resistant coatings from fire residues, *Constr. Build. Mater.*, 2022, 325.
12 S. K. Ho and N. H. Cheung, Sub-Part-per-Billion Analysis of Aqueous Lead Colloids by ArF Laser Induced Atomic Fluorescence, *J. Anal. Chem.*, 2005, **77**(1), 193–199.
13 S. K. Ho and N. H. Cheung, Sensitive elemental analysis by ArF laser-induced fluorescence of laser ablation plumes: Elucidation of the fluorescence mechanism, *Appl. Phys. Lett.*, 2005, **87**(26), 1161.
14 Y. Cai, P. C. Chu, S. K. Ho, *et al.*, Multi-element analysis by ArF laser excited atomic fluorescence of laser ablated plumes: Mechanism and applications, *Front. Phys.*, 2012, **7**, 670–678.
15 N. H. Cheung, Spectroscopy of Laser Plumes for Atto-Mole and ng/g Elemental Analysis, *Appl. Spectrosc. Rev.*, 2007, **42**(3), 235–250.
16 S. K. Ho and N. H. Cheung, Minimally destructive and multi-element analysis of aluminium alloys by ArF laser-induced atomic emissions, *J. Anal. At. Spectrom.*, 2007, **22**(3), 292–297.
17 S. K. Lau and N. H. Cheung, Minimally Destructive and Multi-Element Analysis of Steel Alloys by Argon Fluoride Laser-Induced Plume Emissions, *Appl. Spectrosc.*, 2009, **63**(7), 835–838.
18 S. K. Ho and D. G. Machado, Analysis of Indium Tin Oxide Film Using Argon Fluroide (ArF) Laser-Excited Atomic Fluorescence of Ablated Plumes, *Appl. Spectrosc.*, 2017, **71**(4), 735–743.
19 P. C. Chu, W. L. Yip, Y. Cai, *et al.*, Multi-element analysis of ceramic and polymeric samples by ArF laser excited atomic fluorescence of ablated plumes, *J. Anal. At. Spectrom.*, 2011, **26**(6), 1210–1216.
20 Y. Cai, Z. Huang, M. H. Cheung, *et al.*, Elemental Analysis of Chinese Black Inks on Xuan Paper by ArF Laser-Excited Plume Fluorescence, *Anal. Chem.*, 2016, **88**(22), 10971–10978.
21 S. Carter, A. S. Fisher, M. W. Hinds, *et al.*, Atomic spectrometry update: review of advances in the analysis of metals, chemicals and materials, *J. Anal. At. Spectrom.*, 2013, **28**(12), 1814–1869.
22 J. Peng, F. Liu, F. Zhou, *et al.*, Challenging applications for multi-element analysis by laser-induced breakdown spectroscopy in agriculture: A review, *TrAC, Trends Anal. Chem.*, 2016, **85**, 260–272.
23 X. Wang, Z. Huang, P.-C. Chu, *et al.*, The mechanism of ArF laser-induced fluorescence of dense plume matter, *J. Anal. At. Spectrom.*, 2016, **31**(12), 2363–2374.
24 L. Balazs, R. Gijbels and A. Vertes, Expansion of laser-generated plumes near the plasma ignition threshold, *Anal. Chem.*, 1991, **63**(4), 314–320.
25 S. K. Ho and N. H. Cheung, Sensitive elemental analysis by ArF laser-induced fluorescence of laser ablation plumes: Elucidation of the fluorescence mechanism, *Appl. Phys. Lett.*, 2005, **87**(26), 264104–264107.
26 J. Wang, X. Li, H. Li, *et al.*, Lens-to-sample distance effect on the quantitative analysis of steel by laser-induced breakdown spectroscopy, *J. Phys. D: Appl. Phys.*, 2020, **53**(25), 255203–255212.
27 D. M. Surmick, L. Taleh and N. Melikechi, Effects of Laser Beam Focusing Characteristics on Laser-Induced Breakdown Spectra, *Appl. Spectrosc.*, 2021, **75**(2), 127–136.
28 A. De Giacomo and J. Hermann, Laser-induced plasma emission: from atomic to molecular spectra, *J. Phys. D: Appl. Phys.*, 2017, **50**(18), 183002–183019.
29 R. Sanginés, V. Contreras, H. Sobral, *et al.*, Optimal emission enhancement in orthogonal double-pulse laser-induced breakdown spectroscopy, *Spectrochim. Acta, Part B*, 2015, **110**, 139–145.
30 J. Wang, X. Li, H. Li, *et al.*, Analysis of the trace elements in micro-alloy steel by reheating double-pulse laser-induced breakdown spectroscopy, *Appl. Phys. B: Lasers Opt.*, 2017, **123**(4), 131.
31 J. Wang, H. Fu, Z. Ni, *et al.*, Research on Temporal and Spatial Evolution of Reheating Double-Pulse Laser-Induced Plasma, *Spectrosc. Spectral Anal.*, 2016, **36**(3), 817–822.
32 K. A. Tereszchuk, J. M. Vadillo and J. J. Laserna, Glow-Discharge-Assisted Laser-Induced Breakdown Spectroscopy: Increased Sensitivity in Solid Analysis, *Appl. Spectrosc.*, 2008, **62**(11), 1262.
33 J. Mo, Y. Chen and R. Li, Silver jewelry microanalysis with dual-pulse laser-induced breakdown spectroscopy: 266 + 1064 nm wavelength combination, *Appl. Opt.*, 2014, **53**(31), 7516–7522.
34 V. Contreras, M. A. Meneses-Nava, O. Barbosa-García, *et al.*, Double-pulse and calibration-free laser-induced breakdown spectroscopy at low-ablative energies, *Opt. Lett.*, 2012, **37**(22), 4591–4593.
35 P. Vanraes and A. Bogaerts, Laser-induced excitation mechanisms and phase transitions in spectrochemical analysis – Review of the fundamentals, *Spectrochim. Acta, Part B*, 2021, 179.
36 S. L. Lui and N. H. Cheung, Minimally destructive analysis of aluminum alloys by resonance-enhanced laser-induced plasma spectroscopy, *J. Anal. Chem.*, 2005, **77**(8), 2617–2623.
37 R. E. Russo, X. Mao, J. J. Gonzalez, *et al.*, Laser ablation in analytical chemistry, *Anal. Chem.*, 2013, **85**(13), 6162–6177.
38 Z. Liu, Y. Tian, Y. Lu, *et al.*, Temporal-resolved measurement using a dual light-collection for laser induced breakdown spectroscopy, *Spectrochim. Acta, Part B*, 2021, **180**, 106202.

39 Y.-T. Fu, W.-L. Gu, Z.-Y. Hou, *et al.*, Mechanism of signal uncertainty generation for laser-induced breakdown spectroscopy, *Front. Phys.*, 2021, **16**(2), 22502.
40 R. Sanginés and H. Sobral, Time resolved study of the emission enhancement mechanisms in orthogonal double-pulse laser-induced breakdown spectroscopy, *Spectrochim. Acta, Part B*, 2013, **88**, 150–155.
41 Y. Qiu, A. Wang, Y. Liu, *et al.*, The effect of inter-pulse delay on the spectral emission and expansion dynamics of plasma in dual-pulse fiber-optic laser-induced breakdown spectroscopy, *Phys. Plasmas*, 2020, **27**(8), 083516–083530.
42 K. Rifai, S. Laville, F. Vidal, *et al.*, Quantitative analysis of metallic traces in water-based liquids by UV-IR double-pulse laser-induced breakdown spectroscopy, *J. Anal. At. Spectrom.*, 2012, **27**(2), 276–283.
43 R. Sanginés, H. Sobral and E. Alvarez-Zauco, The effect of sample temperature on the emission line intensification mechanisms in orthogonal double-pulse Laser Induced Breakdown Spectroscopy, *Spectrochim. Acta, Part B*, 2012, **68**, 40–45.
44 B. Y. Cai, X. Mao, H. Hou, *et al.*, Double-pulse laser ablation sampling: Enhancement of analyte emission by a second laser pulse at 213 nm, *Spectrochim. Acta, Part B*, 2015, **110**, 51–55.
45 K. Guo, A. Chen, W. Xu, *et al.*, Effect of sample temperature on time-resolved laser-induced breakdown spectroscopy, *AIP Adv.*, 2019, **9**(6), 065214–065222.
46 A. De Giacomo, R. Gaudiuso, M. Dell'Aglio, *et al.*, The role of continuum radiation in laser induced plasma spectroscopy, *Spectrochim. Acta, Part B*, 2010, **65**(5), 385–394.